Semester Thesis

Influence of Additional Pads on the Electrical Properties of a 3D Transmon

Marco Roth

supervised by
Dr. Simone Gasparinetti

September 25, 2015

Abstract

Transmon qubits confined in three dimensional cavities hold promise for large coherence times which makes them suitable candidates for quantum information processing devices. Many designs today use aluminum as the cavity material which has the disadvantage of making it not possible to tune the Josephson energy with an external magnetic field anymore. Here we investigate the feasibility of fabricating an array of qubits with comparable electrostatic properties on the same sapphire chip. This makes it possible to select which qubit to measure at the end of the fabrication process, while the discarded qubits can be deactivated by physically removing the Josephson junctions. We use numerical simulations (Maxwell) to study how the charging energy and the dipole moment of the selected qubit are modified by the presence of the residual pads. We show that it is possible to keep the charging energy of the qubits at the level of a single qubit while maintaining a minimum dependence on which qubit has actually been chosen as the working qubit.

Contents

1 Introduction

The rapidly developing field of circuit QED has given rise to devices that can produce quantum states with coherence times long enough to allow for quantum information processing (see e.g. [2]).
Transmon qubits that operate at an increased Josephson energy - charging energy ratio E_J/E_c compared to the traditional charge qubit [3] have proven to be capable of maintaining quantum states sufficiently long enough for simple quantum computations . A transmon with carefully tuned E_J/E_c ratio is significantly insensitive to charge noise while the maintained anharmonicity still keeps its quantum states accessible for selective control.
Recently, it has been suggested that the usage of a three-, rather than a two-dimensional cavity, leads to even longer coherence times by enabling increased control over the interaction of the transmon with its environment which constitutes a major source of decoherence for the transmon states [5].

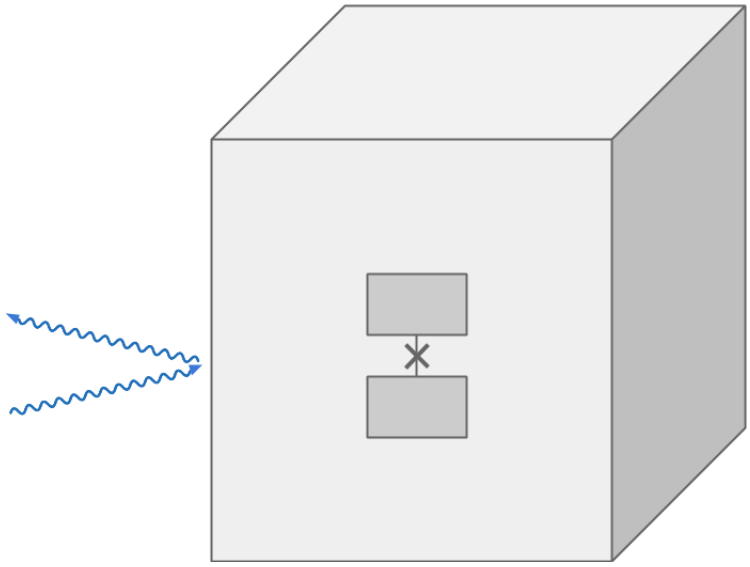

Figure 1: Schematic of a transmon in a 3D cavity. Compared to the 2D Transmon, the electrodes of the qubits are scaled up which lets them act as an antenna with a large dipole moment. Thus sufficient coupling is maintained as this counteracts the decreased electromagnetic field density.

The larger mode volume of a three dimensional cavity can be compensated since the coupling of the qubit to the electromagnetic field is mediated by a large dipole antenna constituted by the electrodes of the qubits (see Figure 1). Thus, despite the reduced electric field produced by a single photon in a 3D environment, the strong coupling regime can be maintained.
One convenient choice of material for the cavity for 3D geometries is Aluminum which shields magnetic fields very efficiently, on the other hand, this makes it impossible to tune the Josephson energy of the qubit by an external magnetic field. Hence, a real time adjustment of the Josephson energy E_J as it is possible for 2D architectures is not possible with Aluminum cavities. It is therefore not longer possible to compensate for deviations from the desired E_J caused by the fabrication process.
In this report, we investigate the feasibility of printing multiple qubits on the sapphire chip, thus increasing the probability of having a qubit with fitting E_J. The idea is to carry out resistance measurements before an experiment that allow one to select the qubit with a Josephson energy that is closest to the ideal value. This qubit would be selected as operating qubit whereas all the other qubits would be physically deactivated by cutting their Josephson junction.
In our simulations, we determine which effects the additional electrically disconnected qubits, that are, once they are disconnected, nothing but pads of metal, have on important parameters such as the

charging energy E_c and the dipole moment (and hence coupling constant g). The simulations were done with the finite element solver 'Maxwell'.

2 Methods

In this chapter, we describe how the parameters of interest are obtained from the simulations. Furthermore, we discuss the setup used in Maxwell and explain how the individual components of the 3D Transmon are modelled.

2.1 Determination of Parameters

Adding more qubits on a chip and destroying them afterwards corresponds to adding pieces of superconducting material right next to the working qubit. This of course is expected to have an influence on working parameters of the qubit. Ideally, we want those parameters, especially the charging energy and the coupling to the cavity modes (and hence the dipole moment as we will see in below), to remain at the level of an isolated qubit even in the presence of other pads.

The coupling constant g can be determined from simulations by considering the electromagnetic field in the cavity. The components of the electric field inside the cavity can be written as [6]

$$E_x = E_{x0} \cos k_x x \sin k_y y \sin k_z z e^{i\omega t} \tag{1}$$
$$E_y = E_{y0} \sin k_x x \cos k_y \sin k_z z e^{i\omega t} \tag{2}$$
$$E_z = E_{z0} \sin k_x x \sin k_y y \cos k_z z e^{i\omega t} \tag{3}$$

with E_{i0} being the amplitude of the respective field component and k_i $(i = x, y, z)$ the components of the wave vector $\mathbf{k}$. The boundary conditions introduced by the walls of the cavity impose restrictions on $\mathbf{k}$. For the field mode (0,1,1) with the lowest frequency, the components of the wave vector satisfy $k_x = 0$ and $k_j = \pi/L_j$ (j = y,z) with L_j being the respective length of the cavity wall. The magnetic field $\mathbf{B}$ can be obtained from Maxwell's equation

$$\nabla \times \mathbf{E} = -\partial_t \mathbf{B}. \tag{4}$$

The total electromagnetic energy is now given by the sum of the integrated electric and magnetic energy densities U_E and U_M which can be obtained from the fields $\mathbf{E}$ and $\mathbf{B}$:

$$E = \int U_E dV + \int U_B dV \tag{5}$$
$$= \frac{1}{2} \int \epsilon_0 \mathbf{E}^2 + \frac{1}{\mu_0} \mathbf{B}^2 dV \tag{6}$$
$$= \frac{1}{8} \epsilon_0 E_0^2 V, \tag{7}$$

where E_0 is the amplitude of the electromagnetic field, V is the volume of the cavity and ϵ_0 is the vacuum permittivity. Since we want to consider the coupling of our qubit to the ground state of the electromagnetic field, we can take E to be the vacuum energy and therefore get

$$\frac{1}{2}\hbar\omega = \frac{1}{8}\epsilon_0 E_0^2 V, \tag{8}$$

which allows us to determine E_0:

$$E_0 = \sqrt{\frac{4\hbar\omega}{\epsilon_0 V}}. \tag{9}$$

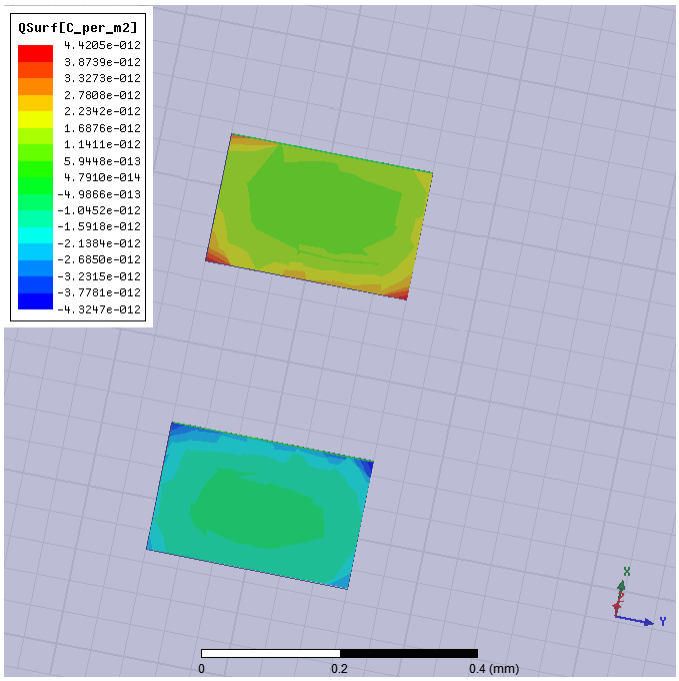

Figure 2: Screenshot taken from Maxwell. It shows the charge distribution for a positively and a negatively charged pad that constitute the electrodes of a single qubit. The charge is mostly concentrated in the corners.

The coupling constant can then be determined by assuming the qubit can be treated like a classical dipole with dipole moment p which leads to

$$g = E_0 p. \tag{10}$$

In this report, we assume that the presence of the additional metal pads on the sapphire chip does not influence E_0 significantly. Thus we mainly investigate the behaviour of the dipole moment when additional pads are added. The dipole moment was calculated by evaluating the volume integral of the charge distribution obtained from Maxwell

$$\mathbf{p} = \int_V dx \rho(x) x. \tag{11}$$

In practice, $\rho(x)$ is obtained by charging the pads of the working qubit with 2e and -2e respectively (see Figure Figure 2). If additional pads are present, they are set to floating,i.e., the charges within the metal are allowed to move freely but they are still neutrally charged.

For most purposes we however use the effective distance d_{eff} between the two center of charges which allows us to compare it with the physical distance between the two pads. It can be obtained from $\mathbf{p}$ by dividing by the total charge.

The charging energy E_{c} is completely determined by the capacitances of the components via

$$E_{\text{c}} = e^2/2C_\Sigma, \tag{12}$$

where C_Σ the total capacitance between the electrodes of the qubit. Therefore it is mainly dependent on the geometry of the setup as well as the spatial relations between the individual elements e.g. the distance and orientation of the pads. The three dimensional geometry leads to a complicated network

of capacitive coupling. The relation between the voltage and the charge of the respective network elements is given by

$$\mathbf{Q} = C\mathbf{V}, \tag{13}$$

where the component Q_i of the charge vector $\mathbf{Q}$ contains the charge of element i. The capacitance matrix C hence relates the charge and voltage vector.

E_c is determined by

$$E_c = \frac{1}{2}\mathbf{Q}^T C^{-1}\mathbf{Q}. \tag{14}$$

were $\mathbf{Q}$ contains the charges 2e (-2e) on the position of the reservoir (island) and the rest is set to 0. The capacitance matrix is obtained from Maxwell.

2.2 Simulations

The experimental setup we used to simulate the behaviour of the system in Maxwell can be seen in Fig. 3. The qubits are simulated as perfectly conducting metal plates. The junction between them is not implemented in the simulation since the length scales within the junction are too small to be simulated in a meaningful way. The capacitance of the junction is however taken into account. In accordance to previous experiments conducted in this group, the capacitance of the Josephson junction C_J is taken to be 10 fF. We add C_J to the element of the capacitance matrix that corresponded to the capacitance between the electrodes of the working qubits before inverting the capacitance matrix. The dimensions of the objects involved can be seen in Table 1.

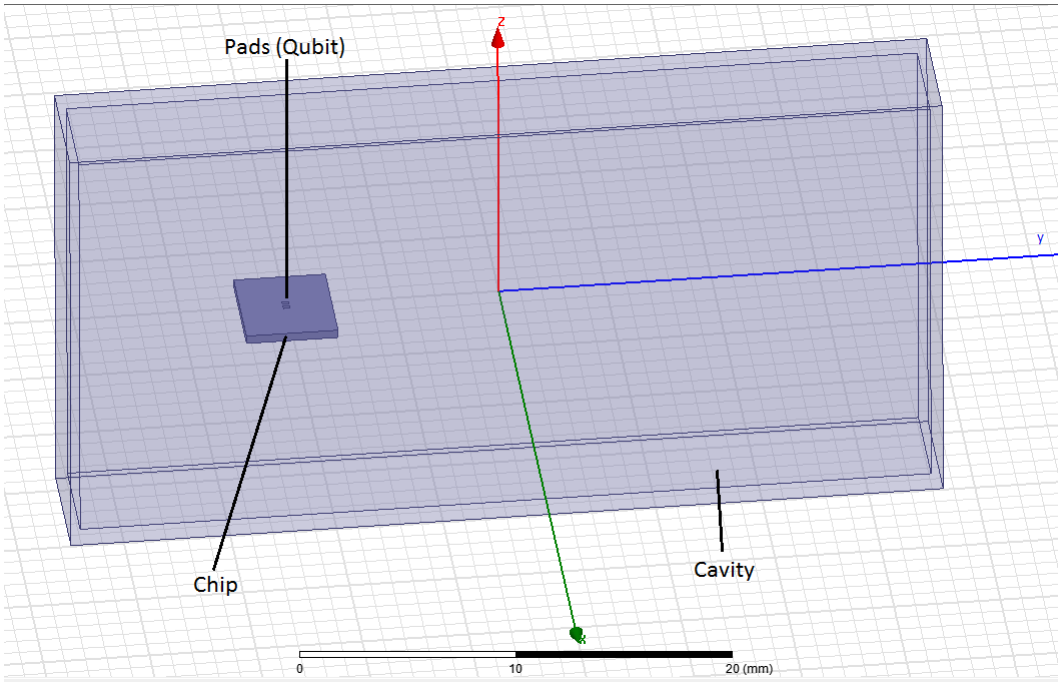

Figure 3: Screenshot taken from Maxwell. In accordance with the real experimental setup, the position of the chip is not in the middle of the cavity but shifted to the side. The qubits are simulated with superdonducting metal plates aligned symmetrically along the y axis.

The situation that we are interested in is the one were all but one qubits are disconnected. These broken qubits are hence just pieces of superconducting metal. We will refer to the qubit that is assumed

Dimensions of objects			Material
Cavity	Δx	5 mm	Superconducter
	Δy	40 mm	
	Δz	20 mm	
Chip	Δx	5 mm	Sapphire
	Δy	4.3 mm	
	Δz	0.4 mm	
Pads	Δx	200 μm	Superconducter
	Δy	300 μm	
	Δz	6 μm	
	Separation	160 μm	

Table 1: Summary of parameters used in the simulations. Some of the parameters like the separation between the electrodes are varied during the optimization process.

to be the one that has not been cut as the *working qubit*. In order to speed up the simulation, we simulate the qubit pads with thickness values of 6 μm compared to the actual size of the order of 100 nm. The results that we obtain this way can be used to get a first, semi quantitative insight into the problem. An analysis of the influence of the pad thickness can be seen in section 4.
When the relative position of the working qubit is changed, we use an index notation to indicate which qubit has been selected. This can be seen in Figure 4.

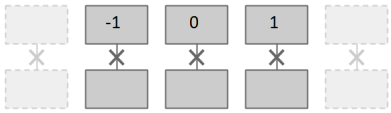

Figure 4: The pads are indexed such that 0 indicates the middle pad and $|i|$ labels the distance from the center.

3 Results

In this chapter we present the results of our simulations. We find that the dipole moment and the charging energy of the working qubit are significantly affected by the presence of additional metal pads. We furthermore discover significant and non-trivial edge effects, in particular a strong dependence of d_{eff} and E_{c} on the relative position of the working qubits with respect to the deactivated qubits. The naive approach of placing many qubits with equal distances fails in achieving a homogeneous distribution of E_{c} and d_{eff} as we show in section 3.1. In chapter 4 we propose an improved design that provides a satisfactory homogeneous distribution of E_{c} and d_{eff} .

3.1 Charging Energy

In a first step, we investigate the behaviour of the parameters of interest by starting with one qubit - the working qubit - and then adding additional pads symmetrically to the left and the right (see Figure 4). The value for a single qubit serves as as reference. We determine it to be $E_{\text{c}}^0 = 423$ MHz. Figure 5 shows the charging energy of a pad located in the center of the sapphire chip as more and more pads are added symmetrically to the left and the right. We observe a variation of up to 10% in E_{c} as the total number of pads is increased from 1 to 9. The strength of the effect is dependent on how the pads are arranged with respect to each other. We see a decrease in E_{c} as more and more pads are added. The effect is stronger for small distances between neighbouring pads. The additional pads introduce additional capacitance to the system which in most cases leads to an overall increased total capacitance C_Σ between the electrodes of the working qubit and therefore a decreased E_{c}. Note however, that this does not need to hold for pads that are situated towards the edge. In section 3.2 this is discussed in detail. The additional capacitance is of course bigger when the distance between the pads is small. As the distance between the pads increases, E_{c} drops less and less when new pads are added. We find that for large enough distances between the qubits (> 60 μm), the charging energy for the center qubit is approximately E_{c}^0.

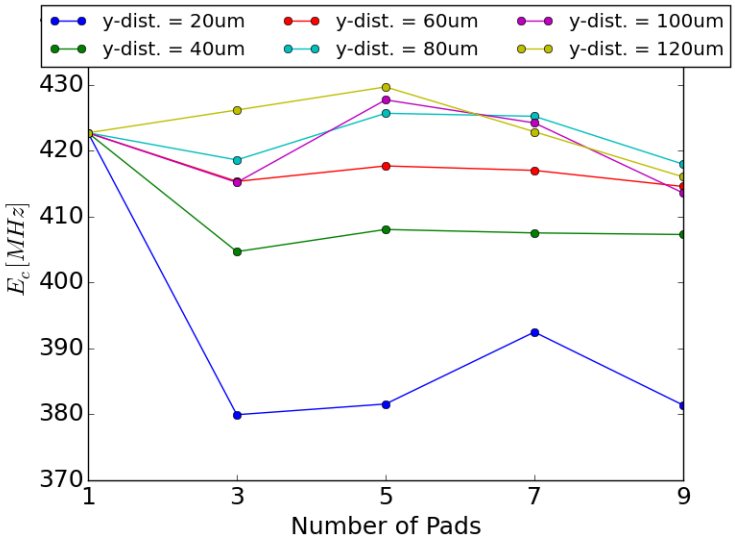

Figure 5: The charging energy E_{c} is shown as a function of the number of pads present on the sapphire chip. The different colors show different distances between neighbouring pads. Every data point is calculated with the working qubit being in the center.

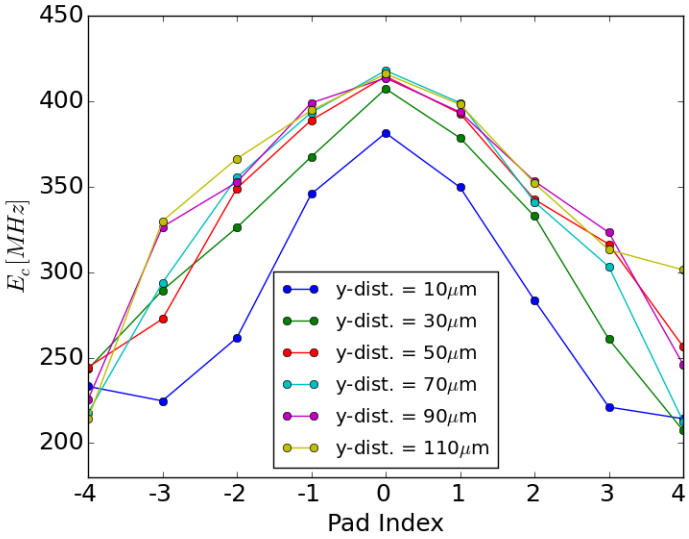

Figure 6: The charging energy E_c is depicted with respect to which qubit is selected to be the working qubit. The qubit position is indexed according to Figure 4.

However, it is not sufficient to maintain E_c for the middle qubit at single qubit level. Since in a real experiment one would not know beforehand which of the written qubits fits our demands of E_J best, we require all of the qubits to deviate not too much from the the baseline level. Figure 6 shows the charging energy as a function of relative position of the working qubit. We find that E_c is indeed dependent on which of the qubits is selected as working qubit as the difference between the center pad and the pads on the edges is now at almost 50% for some cases. The charging energy rapidly decreases as the working qubit is located more to the edge of the capacitive network.

The observed tendency - decreasing charging energy towards the edges with maximum charging energy in the middle is surprising at first sight. You can think of the system as a network of capacitors, dominated by nearest-neighbour interaction. Additional pads add extra capacitance in parallel. However, distant pads should contribute less because they are connected to the middle pads only through a series of capacitors. The pads in the middle are connected through less pads, hence they should get more capacitance. Therefore one would expect the charging energy to be higher at the edges since E_c is inversly proportional to the capacitance. We therefore deem it interesting to further analyze the behaviour of the charging energy of qubits located towards the edges of the qubit array.

3.2 Edge Effects

In order to investigate the edge effects described in the last section, we again vary the relative position of the working qubit - this time with different number of pads present (see Figure 7). We find that with only three pads, the charging energy is indeed larger on the outer qubits than on the middle qubit as we previously expected. However, when more pads are added, the charging energy was less on the edges than in the middle suggesting that other effects play a role.

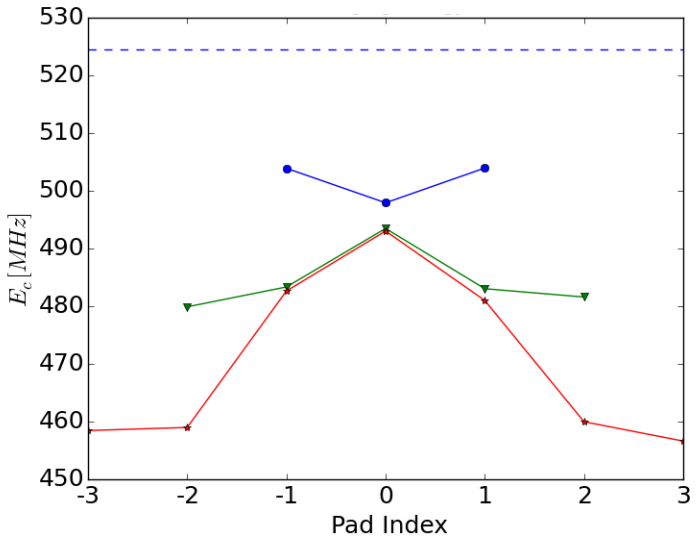

Figure 7: The charging energy is shown for different positions of the working qubit for different total amounts of pads. A qualitative change can be observed when the number is increased from three (blue) to five (green) or seven (red) qubits: Whereas the effect that the total capacitance decreases towards the edges due to the difference of having pads in series rather than in parallel dominates when few pads are simulated, the effect that the element of the capacitance matrix increases towards the edges takes over when the number of pads exceeds five. The dashed line indicates E_c^0.

First, we rule out the possibility that the finite dimensions of the chip itself introduce any effects, i.e., we investigate whether the decrease in E_c comes about when the pads approach the edge of the sapphire chip. We therefore compare simulation results for pads on a chip with realistic dimensions as in Table 1 and chip dimensions much larger. We find (see Figure 8) that the finiteness of the chip indeed influences the charging energy and contributes to the dispersion of the charging energy with respect to the position of the working qubit. But since this effect causes a difference in E_c of about 1% for the outer most pads, we safely neglect it in our further analysis.

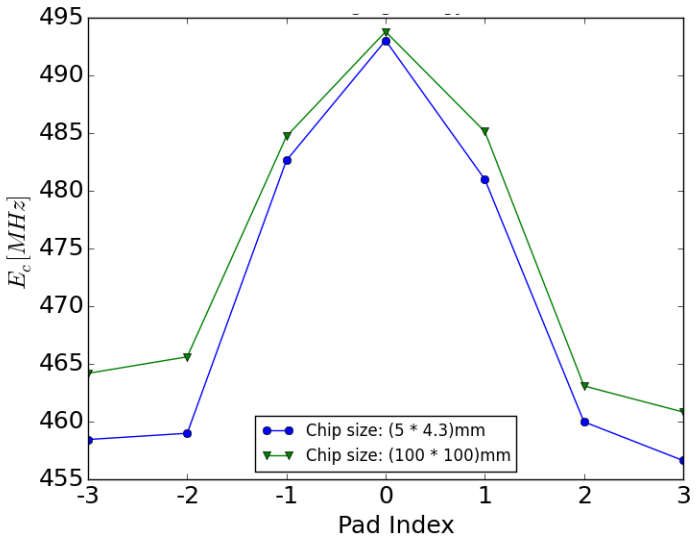

Figure 8: The charging energy of 7 pads are plotted for different dimensions of the chip.

The key effect can be seen if a closer look is taken at the elements of the capacitance matrix (Figure 9). The elements of C that relate pad pairs closer to the edge of the network are significantly bigger than those in the center.

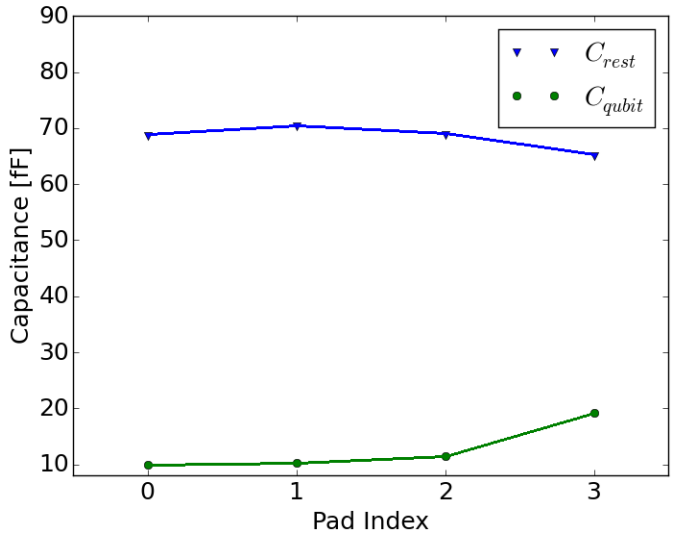

Figure 9: The relation between the matrix element that directly relates the electrodes of the working qubit C_{qubit} and the additional capacitance contributed by the other pads C_{rest} is shown. C_{rest} is obtained via $C_\Sigma = C_{\text{qubit}} + C_{\text{rest}}$. Towards the edges, C_{qubit} contributes significantly more to C_Σ than in the center. This is due to screening effects. This explains the decreasing charging energy towards the edges (see Figure 7).

This is due to the screening between neighbouring pads, causing the electric field towards the edges to be more confined within the gap between the qubit electrodes than in the middle where the field is

more distributed towards the neighboring pads (Figure 10).

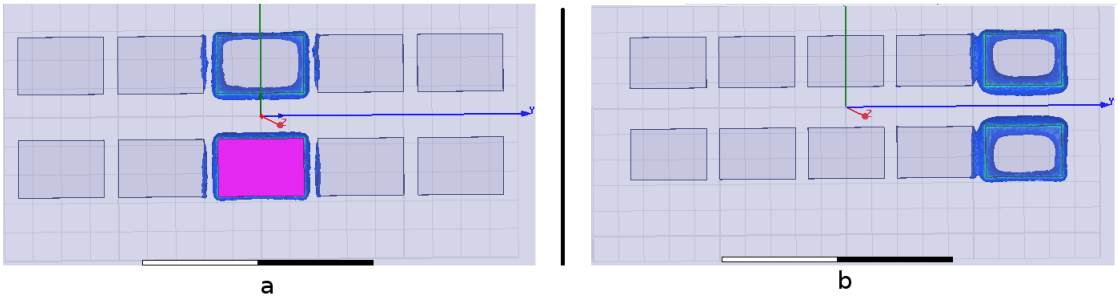

Figure 10: Screenshot taken from Maxwell. The electric field is shown in blue. **a** The figure shows the effect of polarizing the middle qubit by adding a positive charge on the top pad and a negative charge to the bottom pad. **b** The figure shows the right edge qubit selected as working qubit. The field is more confined within the gap between the qubit electrodes in the latter case.

As mentioned earlier, the simulations were conducted with a thickness of the pads of 6 μm. To ensure that our simulation results represent the reality meaningfully, we determined the charging energy and the variation of the charging energy between 7 pads. The results can be seen in Figure 11. From the small effects that can be observed we conclude that the thickness of the pads does indeed not change the qualitative behaviour of our simulations. Note that the results presented in this section were obtained by simulations without a cavity to ensure the behaviour of E_c towards the edges was not an artificial meshing effect.

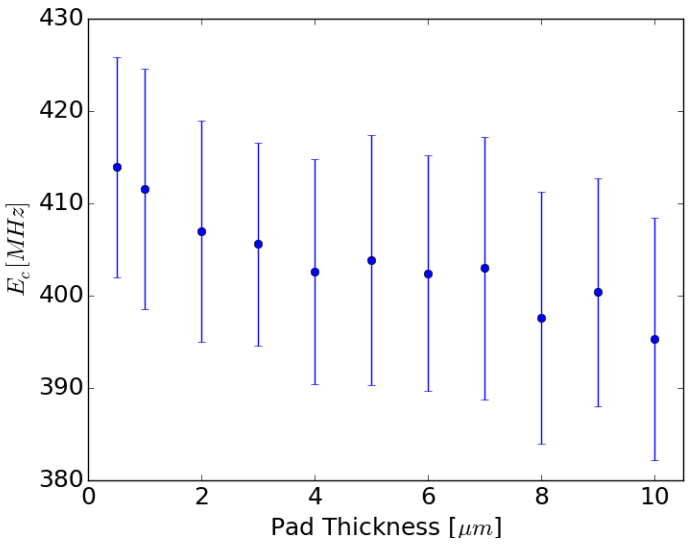

Figure 11: The graph shows the influence of the thickness of the pads. The charging energy of an arrangement of 7 qubits calculated for different sizes of the pads. The error bars are the differences between the highest and lowest value of E_c of the arrangement for a fixed pad thickness. It can be seen that the pad thickness merely introduces a small offset for E_c.

3.3 Dipole Moment

With the method described in section 2.1 we obtain an effective distance between the two center of charges of an isolated single qubit inside a cavity of $d^0_{\text{eff}} = 313.2$ μm. This is smaller than the distance of the two geometrical centers of the pads which is 340 μm which has been used in previous simulations [7]. This smaller distance might explain the discrepancy experienced between simulated coupling constants and previously done experiments [8]. Therefore the method of obtaining the dipole moment by considering the charge distribution suggested in the previous section might lead to more accurate predictions of g in future simulations. Figure 12 shows how d_{eff} evolves with varied distance between the electrodes of a single qubit. It can be seen that d_{eff} approaches the geometrical distance between the center of the two pads for bigger separations between them.

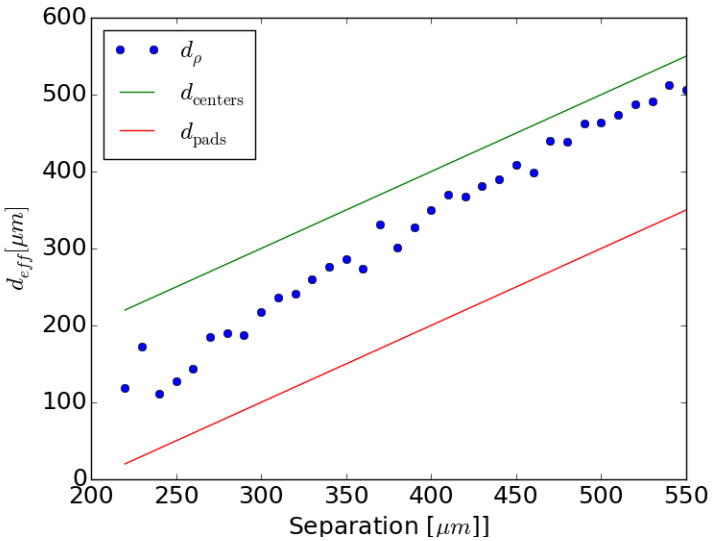

Figure 12: The distance between the center of positive and negative charge (blue dots) is shown in comparison to the distance between the center of mass of the pads (green line) for varying distance between the electrodes. The red line indicates the size of the gap between island and reservoir.

As in the previous section, the effect of adding more pads to the system is investigated (Figure 13). We find a similar dependence on the distance between neighboring qubits as for E_{c}. Small distances invoke large mirror charges between adjacent pads which leads to a decreased dipole moment. An increase in the distance between the pads leads to less mirror effects and therefore a smaller influence on the coupling constant. Since we want to keep the values coupling at about the level of a single qubit, a distance of about 80 μm between the pad seems optimal regarding this aspect for the middle pad.

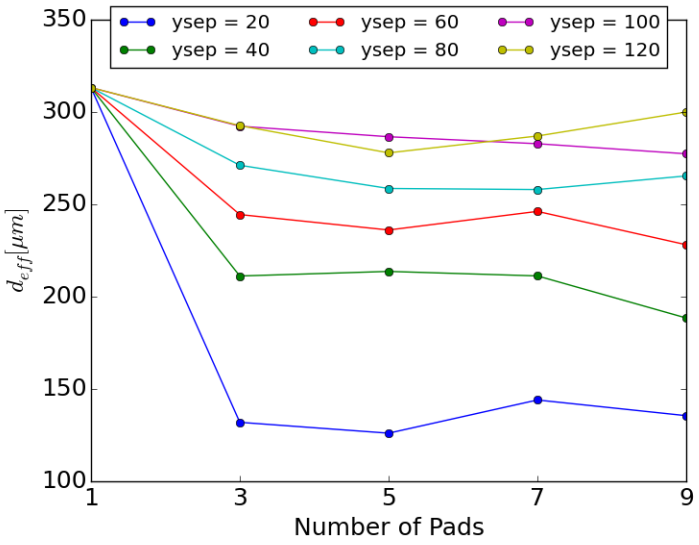

Figure 13: The effective distance between the center of positive and negative charge of the middle qubit is shown for different numbers of pads placed at equal distance between neighboring pads. It can be seen that d_{eff} decreases when the distance between neighboring pads is small. For larger distances, d_{eff} approaches the level of d^0.

4 Towards Optimization: unevenly spaced qubit array

In discussions in sections 3.1 and 3.3 we have seen that the geometrical arrangement of the pads on the sapphire chip influences the dipole moment and the charging energy significantly. We try to carefully adjust the position of the pads such that E_{c} and d_{eff} approach their respective single qubit equivalent E_{c}^0 and d_{eff}^0 regardless of which of the qubits is the designated single working qubit. We therefore run several simulations with varying distances between adjacent pads to determine an optimal set of distance values. The final set of parameters for the prototype can be seen in Table 2.

a	200 μm
b	300 μm
c	260 μm
d_{12}	50 μm
d_{23}	70 μm
d_{34}	200 μm

Table 2: Summary of parameters used in the simulations. Some of the parameters like the separation between the electrodes are varied during the optimization process. d_{ij} is the distance between pad i and j. The parameters a, b, c are the dimensions of the qubit (see Figure 14).

In the final setup, five qubits with increasing qubit to qubit distance from the middle towards the edge pads are used. An additional set of pads is added next to each of the outer qubits in order to screen the electric field of the outer qubits in order to decrease their capacitance and increase their charging energy. After an optimal spacing in the y direction is found, the separation between the two qubit electrodes in the x direction is increased until E_{c} matches the values of a single qubit. This has to be done to account for the additional capacitance added to the system by the unused and destroyed qubits. The distribution of E_{c} and d_{eff} for a design that exhibits a maximum variation of 12% for E_{c}

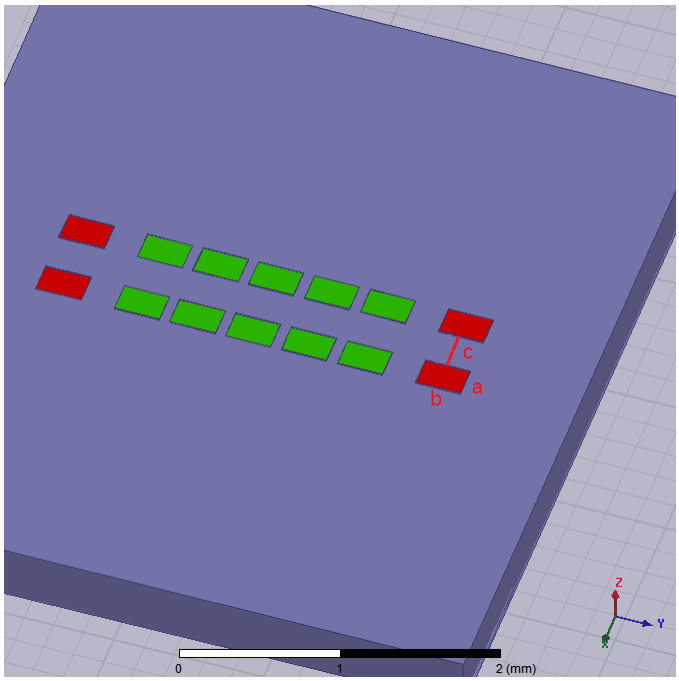

Figure 14: Screenshot from Maxwell of the setup that minimized the variation in E_c. The green pads are real qubits whereas the red pads are only metal plates that decrease the capacitance of the outer qubits relative to the inner qubits in order to make the distribution of E_c more homogeneous.

and 10% for d_{eff}. The result can be seen in Figure 15. Note that d_{eff} stays above the single qubit value for all of the pads such that the coupling to the field is enhanced in this particular design.

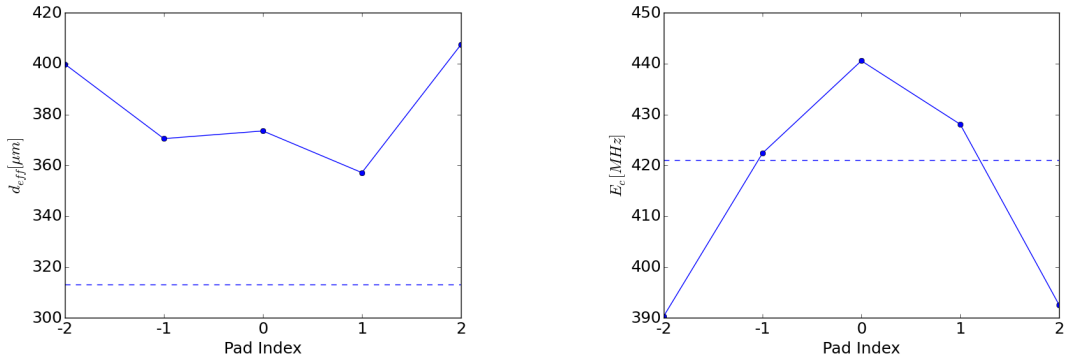

Figure 15: d_{eff} (left) and E_c (right) are shown for the simulated optimal setup. The value of the respective parameter for a single qubit is depicted as a dashed line. d_{eff} and thus the dipole moment are constantly above the the level of the single qubit. Thus a sufficiently strong coupling can be maintained in this approach. The strong coupling is a result of the - compared to the single qubit case - larger distance between the pads within one qubit which had to be introduced to keep the charging energy at around 420 MHz.

5 Conclusion

In this report we demonstrate the feasibility of having multiple qubits on one sapphire chip with the purpose of using the most suitable one for experiments. Important parameters like the charging energy and the dipole moment can be maintained within 12% to the respective single qubit values by engineering the geometrical properties of the qubits. To make the distribution of parameters even more uniform, it is possible to exploit additional degrees of freedom which have not been investigated here. It is e.g. conceivable to individually adjust the distance between the electrodes within one qubit or to tune the size of the pads as needed.
Planned experiments with a prototype qubit will have to show whether the approach that has been investigated here can produce useful results. There are still open questions like how the process of physically cutting the junction of a qubit might be done without affecting the coherence properties of the qubit. However, if the presented approach proves to be successful, it might provide a significant speed-up for future experiments with a 3D geometry as the efficiency of the lengthy fabrication process of the qubits can be drastically increased by having more than just one possibility of having the right set of parameters.

References

[1] J. Clarke et al. *Superconducting quantum bits* Nature 453, 1031 (2008)

[2] Devoret, M. and Schoelkopf, R. J., *'Superconducting Circuits for Quantum Information: An Outlook* Science 339, 1169-1174 (2013)

[3] J. Koch et al. *Charge-insensitive qubit design derived from the Cooper pair box* Physical Review A 76, 042319 (2007)

[4] L. DiCarlo et al. *Demonstration of two-qubit algorithms with a superconducting quantum processor* Nature 460, 7252 (2009)

[5] H. Paik et al. *Observation of High Coherence in Josephson Junction Qubits Measured in a Three-Dimensional Circuit QED Architecture* Physical Review Letters 107, 240501 (2011)

[6] A. Wolski *Lecture Notes on Advanced Electromagnetism* PHYS370–Advanced Electromagnetism, University of Liverpool, `http://pcwww.liv.ac.uk/~awolski/main_teaching_Liverpool_PHYS370.htm`

[7] S. Berger *Vacuum-inducted Berry phase project* Workbook no. VIII and Mathematica files, (2014)

[8] S. Gasparinetti *Vacuum-induced Berry phase project* Workbook no. 1 and related paper, (2014/2015)

Eidgenössische Technische Hochschule Zürich
Swiss Federal Institute of Technology Zurich

Declaration of originality

The signed declaration of originality is a component of every semester paper, Bachelor's thesis, Master's thesis and any other degree paper undertaken during the course of studies, including the respective electronic versions.

Lecturers may also require a declaration of originality for other written papers compiled for their courses.

I hereby confirm that I am the sole author of the written work here enclosed and that I have compiled it in my own words. Parts excepted are corrections of form and content by the supervisor.

Title of work (in block letters):

Authored by (in block letters):
For papers written by groups the names of all authors are required.

Name(s):	**First name(s):**

With my signature I confirm that

- I have committed none of the forms of plagiarism described in the 'Citation etiquette' information sheet.
- I have documented all methods, data and processes truthfully.
- I have not manipulated any data.
- I have mentioned all persons who were significant facilitators of the work.

I am aware that the work may be screened electronically for plagiarism.

Place, date	**Signature(s)**

For papers written by groups the names of all authors are required. Their signatures collectively guarantee the entire content of the written paper.